ORNL/LTR-2023/2888

High-Temperature Creep Behavior of Thin-walled FeCrAl Alloy Tubes

Nuclear Technology Research and Development

Prepared for
U.S. Department of Energy
Nuclear Technology R&D
Advanced Fuels Campaign

David T. Hoelzer, Dustin Heidel,
Yukinori Yamamoto, Caleb P. Massey
Oak Ridge National Laboratory

May 31, 2023
M3FT-23OR020202022

DISCLAIMER

This information was prepared as an account of work sponsored by an agency of the U.S. Government. Neither the U.S. Government nor any agency thereof, nor any of their employees, makes any warranty, expressed or implied, or assumes any legal liability or responsibility for the accuracy, completeness, or usefulness, of any information, apparatus, product, or process disclosed, or represents that its use would not infringe privately owned rights. References herein to any specific commercial product, process, or service by trade name, trade mark, manufacturer, or otherwise, does not necessarily constitute or imply its endorsement, recommendation, or favoring by the U.S. Government or any agency thereof. The views and opinions of authors expressed herein do not necessarily state or reflect those of the U.S. Government or any agency thereof.

ACKNOWLEDGMENTS

This research was sponsored by the Advanced Fuels Campaign Program of the US Department of Energy (DOE) Office of Nuclear Energy. The authors would like to acknowledge T.S. Byun and Ben Garrison for their insightful technical reviews. The report was authored by UT-Battelle LLC under Contract No. DE-AC05-00OR22725 with DOE.

SUMMARY

This report summarizes measured creep properties for FeCrAl alloy C26M measured using subsized specimens machined from prototypic thin-walled tubes. A representative tube fabricated in a previous large-batch production effort was machined into dual-gauge axial specimens using electrical-discharge machining. Creep tests, comprising strain-rate jump tests (SRJ), jump stress (JS) and constant-stress (CS) tests, were conducted at temperatures ranging from 600-900ºC to determine creep mechanisms (elucidated from stress exponents) and activation energies to compare with prior data available in the literature at temperatures up to 650ºC. It was found that the results from the SRJ tests indicated that the highest stress exponent of 5.8 occurred at 600ºC, which decreased to the lowest stress exponent of 2.5 at 700ºC. At higher temperatures, the stress exponents increased slightly to a range of 2.9 to 4.3 between 750ºC and 900ºC. The high stress exponent value of 5.8 suggested dislocation glide creep mechanisms dominated creep deformation at 600ºC since high stress values were measured. The low stress exponent of 2.5 at 700ºC suggested diffusional creep mechanisms start to occur that aid in dislocation cross-slip and climb mechanisms. The slightly higher stress exponents of 2.9 to 3.9 may suggest different contributions of creep deformation mechanisms based on diffusional processes associated with Nabarro-Herring and Coble creep and dislocation creep that involve thermally activated cross-slip and climb mechanisms. These deformation mechanisms could have also been affected by the development of recovery and/or recrystallization processes in the microstructure of the C26M2 specimens. From the SJ and single CS tests, two sets of creep activation energies were calculated. The steady state creep values obtained from the SJ tests showed several abnormalities especially with the data at 850ºC. The comparison of the creep activation energies between the data from the SJ and CS tests showed higher creep rates for the SJ tests than the CS tests, indicating microstructure softening occurred in the C26M2 specimens during the SJ tests that led to the higher creep rates at stresses above the initial stress of 10 MPa. For the CS tests, the results showed steady increases in MCR with increasing temperature at each stress. The best linear fit to the MCR values at each stress was with data obtained at 800ºC, 850ºC and 900ºC. The lowest Q_c value of 130.8 KJ/mole was observed with the highest stress of 25 MPa. As stress was lowered, the Q_c values increased continuously to the highest value of 188.2 KJ/mole at 10 MPa. This trend suggests that the dominant creep mechanism is diffusional based dislocation climb since the decreasing activation energies with increasing stress promotes easier dislocation climb around obstacles. The comparison between the SJ and CS tests indicates that the best type of creep test performed on FeCrAl alloys such as C26M2 is the single CS test.

CONTENTS

Page

ACKNOWLEDGEMENTS v
SUMMARY vii
CONTENTS ix
FIGURES xi
TABLES xiii
1. INTRODUCTION 1
2. BACKGROUND 1
   2.1 Burst Tests 1
   2.3 Creep Tests 3
3. EXPERIMENTALPROCEDURES 6
   3.1 Material 6
   3.2 Samples 7
   3.3 Creep Tests 8
      3.3.1 Creep Concepts 8
      3.3.2 Grips 9
      3.3.3 Test Frame 9
      3.3.4 Test Conditions 10
   3.4 Strain Rate Jump Tests 11
   3.5 Stress Jump and Constant Stress Tests 12
4. RESULTS AND DISCUSSION 14
   4.1 Strain rate jump tests 14
   4.2 Stress jump and constant stress test 16
   4.3 Accuracy of the creep testing methods 18
5. SUMMARY 22
6. FUTURE WORK 23
7. REFERENCES 23

FIGURES

FIGURE		PAGE
Figure 1.	The burst temperature as a function of engineering hoop stress of first generation FeCrAl cladding (C35: Fe-13Cr-5Al-0.5Y and C54: Fe-15Cr-4Al-0.5Y) [1].	1
Figure 2.	Experimental data for axial tube specimens of C35 and the best fit for burst criteria [2].	1
Figure 3.	Experimental vs. simulated burst conditions for thin-walled C26M tubes. Experimental data from Bell et al. [3] and simulated data from Sweet et al. [4].	1
Figure 4.	Uniaxial tensile creep tests performed on C35 FeCrAl alloy at 800ºC [1].	2
Figure 5.	Compilation of creep test conditions from studies of FeCrAl alloys including the current study of C26M2 [1,2,5,6]..	3
Figure 6.	Design illustrations of the initial and modified dual gauge axial specimen for the thin wall tube of C26M2. (a) initial design, (b) modified design and (c) plug for modified design	4
Figure 7.	Digital images of each type of dual gauge specimens fabricated from the thin wall tube of C26M2. (a) initial design, (b) fully assembled modified design specimen.	5
Figure 8.	Plots illustrating the stress-strain curves for (a) creep tests using a constant stress and (b) creep tests using a constant strain rate.	7
Figure 9.	The specimen grips used for the dual gauge axial specimens..	10
Figure 10.	The set up of an axial specimen on the Instron 4204 tensile frame heated by induction furnace. (a) the axial specimen with the attached thermocouple loaded in the grips and (b) placement of the ceramic shield covering the axial specimen and grips prior to heating to the test temperature...	11
Figure 11.	Stress-strain curve obtained from the SRJ test on the axial specimen of C26M2 at 800ºC...	12
Figure 12.	The stress jump test conducted on axial specimens of C26M2 showing the relationship between strain and time for each region of constant stress at 10, 15 and 20 MPa at 800ºC...	13
Figure 13.	The constant stress test conducted on axial specimens of C26M2 showing the relationship between strain and time for constant stress at 800ºC and 20 MPa. ...	14
Figure 14.	Comparison of the thermal creep behavior of 14YWT with OFRAC from SRJ tests conducted on axial specimens at 800ºC. The calculated stress exponents (n) are shown for each set of creep data...	15
Figure 15.	The constant stress test conducted on axial specimens of C26M2 showing the relationship between strain and time for constant stress at 800ºC and 20 MPa.	16
Figure 16.	Results of the stress jump tests conducted at stresses of 10, 15 and 20 MPa for temperatures of 800ºC, 850ºC and 900ºC..	17
Figure 17.	Results of the constant stress tests conducted at stresses of 10, 15, 20 and 25 MPa for temperatures of 750ºC, 800ºC, 850ºC and 900ºC.	18
Figure 18.	Comparison of the MCR values obtained from the constant stress tests and the stress jump tests (enclosed open circles and black arrow for 15 MPa SJ) for stresses of 10, 15, 20 and MPa for temperatures of 800ºC, 850ºC and 900ºC....	19
Figure 19.	Compilation of the stress exponents obtained from the strain rate jump tests over the temperance range of 600ºC to 900ºC and the MCR values measured in the constant stress tests 800ºC, 850ºC and 900ºC.	20

TABLES

TABLE **PAGE**

Table 1. Summary of the stresses and temperatures and the measured secondary creep rates for creep tests conducted on FeCrAl C26M2, C35M, C35M2 and C35MN2 alloys.. 5

Table 2. Temperature, initial strain rate and stress value at the initial strain rate that were used in the strain rate jump tests on the dual gauge axial specimens... 11

Table 3. The values of constant stress used at each temperature in the stress jump and constant stress tests on the dual gauge axial..... 11

Table 4. Test parameters that were used and the values of either constant stress (SRJ) or steady state creep rate (CS) that were measured for calculation of the stress exponent (n)..... 21

Table 5. Test parameters for the single constant stress (CS) tests and the values of minimum creep rate (CS) that were measured for calculation of the activation energy of creep (Qc)..... 22

1. INTRODUCTION

FeCrAl alloys are currently being developed for use in light water reactors as a potential accident tolerant fuel (ATF) cladding that can help mitigate deleterious phenomena associated with design basis (and beyond design basis) accident scenarios. One of these scenarios is a loss-of-coolant accident (LOCA), which in its most severe form entails a double guillotine break in the cold legs (primary coolant pathways) running to the reactor pressure vessel. In this scenario, the temperature of the fuel/cladding elements increases over time as residual decay heat (and heat generated due to exothermic oxidation reactions) is unable to be removed by the near adiabatic thermal boundary condition. The pressurized nature of these tubes, coupled with the increasing cladding temperature, leads to ballooning of the cladding and eventual failure via pressurized burst. To better understand the balloon and burst event, it is important to understand both the elasto-plastic response of the FeCrAl alloy in addition to the effects of high-temperature creep in LOCA-relevant regimes.

In this study, the creep behavior of C26M2 FeCrAl is investigated at temperatures and stresses that are representative of severe accident conditions. Therefore, the background section will cover previous FeCrAl studies of the balloon and burst behavior and the temperature dependence of creep properties of four different FeCrAl alloys. The creep properties of C26M2 will be obtained from strain rate jump (SRJ) tests to determine the stress exponents and both stress jump (SJ) and constant stress (CS) tests to ascertain the creep activation energies at stresses and temperatures leading to cladding burst conditions for FeCrAl alloys. Understanding the creep behavior of C26M2 will allow qualitative interpretations of the cladding burst behavior and will contribute important creep parameters to the BISON fuel performance code.

2. BACKGROUND

2.1. Burst Tests

The out-of-pile burst tests of thin wall tubes of first generation model FeCrAl alloys (C35: Fe-13Cr-5Al-0.5Y and C54: Fe-15Cr-4Al-0.5Y) was investigated by Massey et al. [1]. The tube geometry of C35 and C54 were 9.50 mm outside dimension (OD), 8.73 mm inside dimension (ID) with a wall thickness of 385 μm. The burst tests were conducted at Severe Accident Test Station at Oak Ridge National Laboratory (ONRL). The tube samples were 30 cm long and were internally pressurized with helium and heated using an infrared furnace with flowing steam under atmospheric pressure on the exterior surface of the tube during the burst test. The engineering hoop stress was determined following the post-test analysis of the tube sample. Figure 1 shows the plot of temperature as a function of hoop stress for the burst tests for C35 and C54. The results indicated that the tube burst conditions of the two FeCrAl alloys occurs over the temperature range of ~700 to ~1300ºC and hoop stress range of ~16 to ~138 MPa.

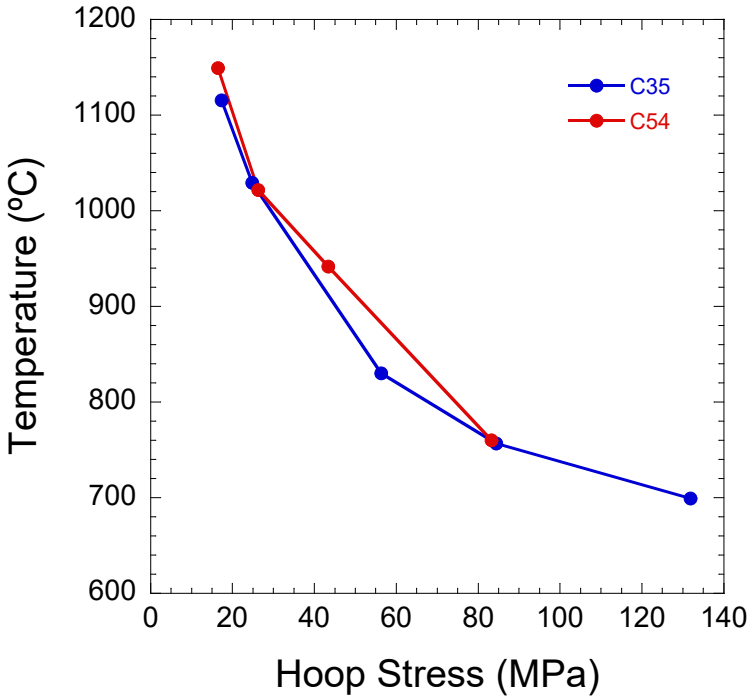

Figure 1. The burst temperature as a function of engineering hoop stress of first generation FeCrAl cladding (C35: Fe-13Cr-5Al-0.5Y and C54: Fe-15Cr-4Al-0.5Y).

The development of a burst stress (σ_{burst}) model for FeCrAl alloy cladding that varies as a function of temperature was determined by Gamble et al. [2]. Using the burst data for C35 obtained by Massey et al. [1], the experimental values of burst stresses were determined to decrease following an exponential decay with increasing temperatures consistent with $\sigma_{burst} = 28{,}440.98e^{-0.005588T}$, where T is temperature. Figure 2 shows the plot of the experimental data and best fit for determining the burst criteria for C35.

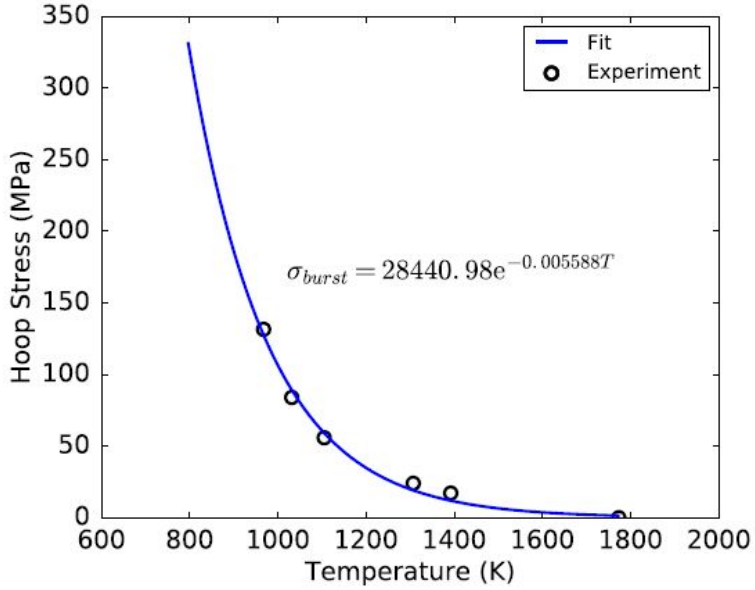

Figure 2. Experimental data for axial tube specimens of C35 and the best fit for burst criteria [2].

Although our understanding of the burst properties of FeCrAl alloys is improving, recent simulation results indicate gaps still exist in our ability to predict deformation behavior at higher temperatures. For instance, Bell et al. [3] have recently provided burst data for thin-walled tubes of C26M, which are plotted below in Figure 3. Overlaid atop this plot are recent BISON simulations of predicted burst conditions using the same experimental pressure/temperature/time data available from the experiments [4]. From the BISON modeling, it was found that although burst can be effectively predicted at higher hoop stresses, larger discrepancies exist at lower stress/higher temperature conditions. Thus, an opportunity exists to begin mapping higher temperature (>650C) thermal creep regimes for the FeCrAl alloy system in an effort to begin explaining the origins of these potential gaps in modeling capabilities.

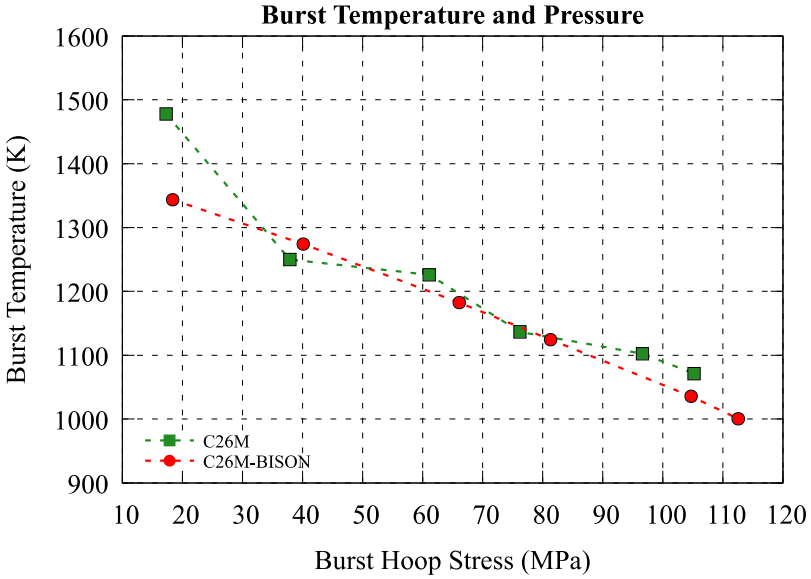

Figure 3. Experimental vs. simulated burst conditions for thin-walled C26M tubes. Experimental data from Bell et al. [2] and simulated data from Sweet et al. [3].

2.2 Creep tests

Thermal creep tests have been conducted on tensile specimens of FeCrAl alloys designated as C35M2 (13.06Cr - 5.15Al - 1.97Mo - 0.12Si - 0.10Y) and C35MN5 (13.02Cr - 5.08Al - 1.99Mo - 0.21Si - 0.97Nb - 0.032Y) by Terrani et al. [5]. The C35M2 alloy was hot forged at 650ºC from a 3.6 cm diameter round bar to a 1.6 cm squarer bar. The C35MN5 alloy was hot extruded at 800ºC from a 2.9 inch diameter rod to a 1.0 inch diameter rod followed by annealing for 1 h at 800ºC. Out-of-pile creep tests were conducted on unirradiated specimens at 350ºC in an inert gas atmosphere. The stresses used in the thermal creep tests were 300 MPa and 325 MPa, which were selected to represent the stresses the develop in thin wall cladding under fuel pin operation. The thermal creep tests lasted ~1 week, or 168 h. For C35M2, the thermal creep rates were 1.2 x 10^{-6}/h at 300ºC and 2.9 x 10^{-6}/h at 325ºC. The thermal creep rates for C35MN5 were 1.0 x 10^{-6}/h at 300ºC and 3.4 x 10^{-6}/h at 325ºC. These values of creep rates for C35M2 and C25MN5 do not show a significant advantage with composition differences, but that different deformation processing may have played a minor role on the creep properties.

The only creep tests that have been conducted with stresses and temperatures relevant to burst conditions or FeCrAl alloys was the study by Massey et al. [1]. The creep tests were performed on the C35MN (Fe-13Cr-4.5Al-2Mo-1Nb-0.25Y-0.2Si) FeCrAl alloy using dog bone specimens with gauge section of 2 x 2 mm. Two creep tests were conducted at 800ºC and applied stresses of 20 and 25 MPa. Figure 4 shows by

permission the creep curves obtained from the two creep tests [1]. The results shows a steady state creep rate of 1.6×10^{-7} s^{-1} at 20 MPa and 2.5×10^{-6} s^{-1} at 26 MPa.

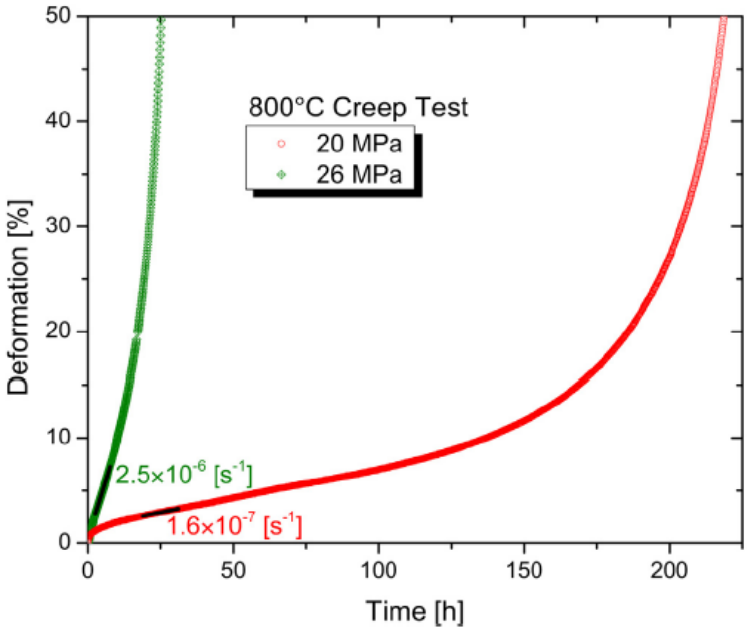

Figure 4. Uniaxial tensile creep tests performed on C35 FeCrAl alloy at 800ºC [1].

Burst tests were conducted on FeCrAl C26M2 tubing to study the stress-rupture behavior in the temperature range of 480 - 650ºC by Joshi et al. [6]. For these tests, the tubes were internally pressurized with Ar gas and held at elevated temperatures until failure occurred. A series of burst tests consisting of multiple internal pressures were conducted at temperatures of 480, 510, 540, 570, 600 and 650ºC. The hoop stress was calculated for each internal pressure condition and correlated with the rupture time. The temperatures and hoop stresses for each burst test in this study are shown in Table 1. Inspection of the ruptured tubes revealed two types of failure modes: direct open rupture and small crack and pinhole fracture with little to no ballooning. By analyzing the rupture data, the steady state strain rates were obtained and used to calculate the stress exponent and activation energy of C26M2.

Figure 5 shows the compilation of the creep results obtained from the limited number of studies on FeCrAl alloys [1,5,6]. From the log σ versus test temperature, the results can be separated into three regions representing the upper operating conditions for a light water reactor, the intermediate stresses and temperatures between the reactor operating conditions and the stresses and temperatures for fuel cladding burst conditions. The test conditions used in this work are shown in this figure with red squares. The goal of this work is to investigate the creep behavior of C26M2 using strain rate jump, stress jump and single constant stress tests to obtain stress exponents and creep activation energies at stresses and temperatures leading to fuel cladding bursts. Table 1 summarizes the stresses and temperatures and the measured secondary creep rates for creep tests conducted on FeCrAl C26M2, C35M, C35M2 and C35MN2 alloys [1,5,6].

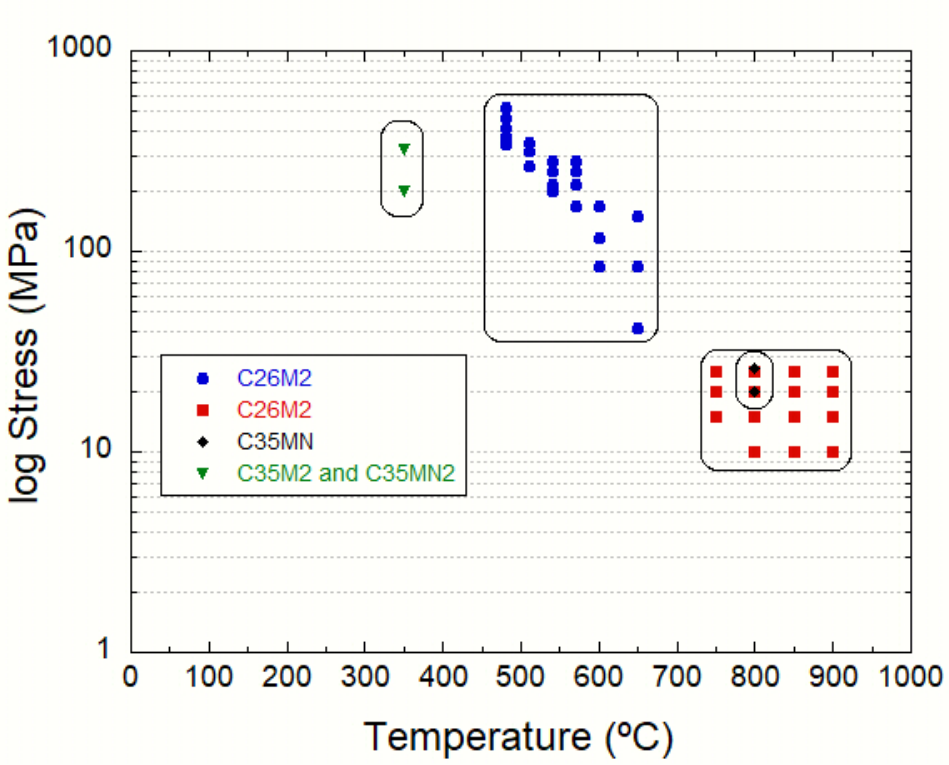

Figure 5. Compilation of creep test conditions from studies of FeCrAl alloys including the current study [1,5,6].

Table 1. Summary of the stresses and temperatures and the measured secondary creep rates for creep tests conducted on FeCrAl C26M2, C35M, C35M2 and C35MN2 alloys.

Alloy Code	Temperature (ºC)	Stress (MPa)	Secondary Creep Rate (s^{-1})	Reference
C26M2	480	342.2	1.40×10^{-7}	[6]
	480	350.2	1.70×10^{-7}	
	480	375.6	2.40×10^{-7}	
	480	417.4	1.80×10^{-6}	
	480	467.4	2.50×10^{-6}	
	480	517.5	6.40×10^{-6}	
	510	267.1	1.70×10^{-7}	
	510	317.2	5.40×10^{-7}	
	510	350.6	9.10×10^{-7}	
	540	200.3	1.60×10^{-7}	
	540	204.5	1.90×10^{-7}	
	540	217.0	4.50×10^{-7}	
	540	250.4	1.20×10^{-6}	
	540	283.8	3.70×10^{-6}	
	570	166.9	8.20×10^{-7}	
	570	217.0	2.00×10^{-6}	
	570	250.4	7.00×10^{-6}	
	570	283.8	6.40×10^{-6}	
	600	83.5	5.30×10^{-7}	
	600	116.9	9.60×10^{-7}	
	600	166.9	1.10×10^{-6}	
	650	41.7	5.70×10^{-8}	
	650	83.5	1.20×10^{-6}	
	650	150.2	4.60×10^{-6}	
C35MN	800	20	2.5×10^{-6}	[1]
	800	26	1.6×10^{-7}	
C35M2	350	300	3.33×10^{-10}	[5]
	350	325	8.06×10^{-10}	
C35MN2	350	300	2.78×10^{-10}	[5]
	350	325	9.44×10^{-10}	

3. EXPERIMENTAL PROCEDURES

3.1. Material

The thin wall tube used in this study was produced as the third “large batch” production of C26M at ORNL under the AFC program. The master ingots were produced by Sophisticated Alloys via vacuum induction melting followed by hot-isostatic pressing. The heat number of the master ingot was 17025001. The ingots were straightened, annealed, and centerless ground followed by gun drilling to produce master tubes. The thin wall tubes were warm drawn with a mandrel using multiple area reduction plus annealing passes to the final geometries by Century Tubes, Inc. The final tube lengths were ~68 inches. Both PWR and BWR tube geometries were produced, but the alloy referenced in this work uses the PWR geometry. The heat designation of the C26M2 thin wall tube used in this work was BA2-B.

3.2 Samples

Both dual gauge axial and dual gauge ring specimens were fabricated from the thin wall tube of C26M2. There was a design modification in the dual gauge axial specimens implemented after the strain rate jump testing to minimize distortion in the gauge head under constraint of the grips with increasing crosshead displacement. The initial and modified designs of the dual-gauge axial specimen for the thin wall tube of C26M2 are shown in Figure 6. Orthogonal views of the initial axial and the modified axial specimens are shown in Figures 6a and 6b, respectively. For the initial axial specimen, the dimension of the gauges was 4 mm long and 2 mm wide with a 4 mm long gauge head. For the modified axial specimen, the dimension of the gauges was 4 mm long and 2 mm wide with a 7 mm long gauge head and a 3 mm diameter hole bored near the mod-section of the gauge head on opposite sides of the tube 90ºC rotation from each gauge. This design included a plug shown in Figure 6c that contained a hole bored through the plug at mid-section in height. Small 316 stainless steel screws of 12 mm length fastened the plug to each gauge head and secured with small hex nuts. The thickness of the gauge head for both axial specimen designs was nominally 0.6 mm based on the wall thickness of the thin wall tube of C26M2. Therefore, the gauge width has a slight curvature of $2\pi r$. Both axial specimen designs have 1 mm radius shoulders (R1) at the base of the gauge where it meets the gauge head. This design permitted shoulder loading during the SRJ, SJ and CS tests.

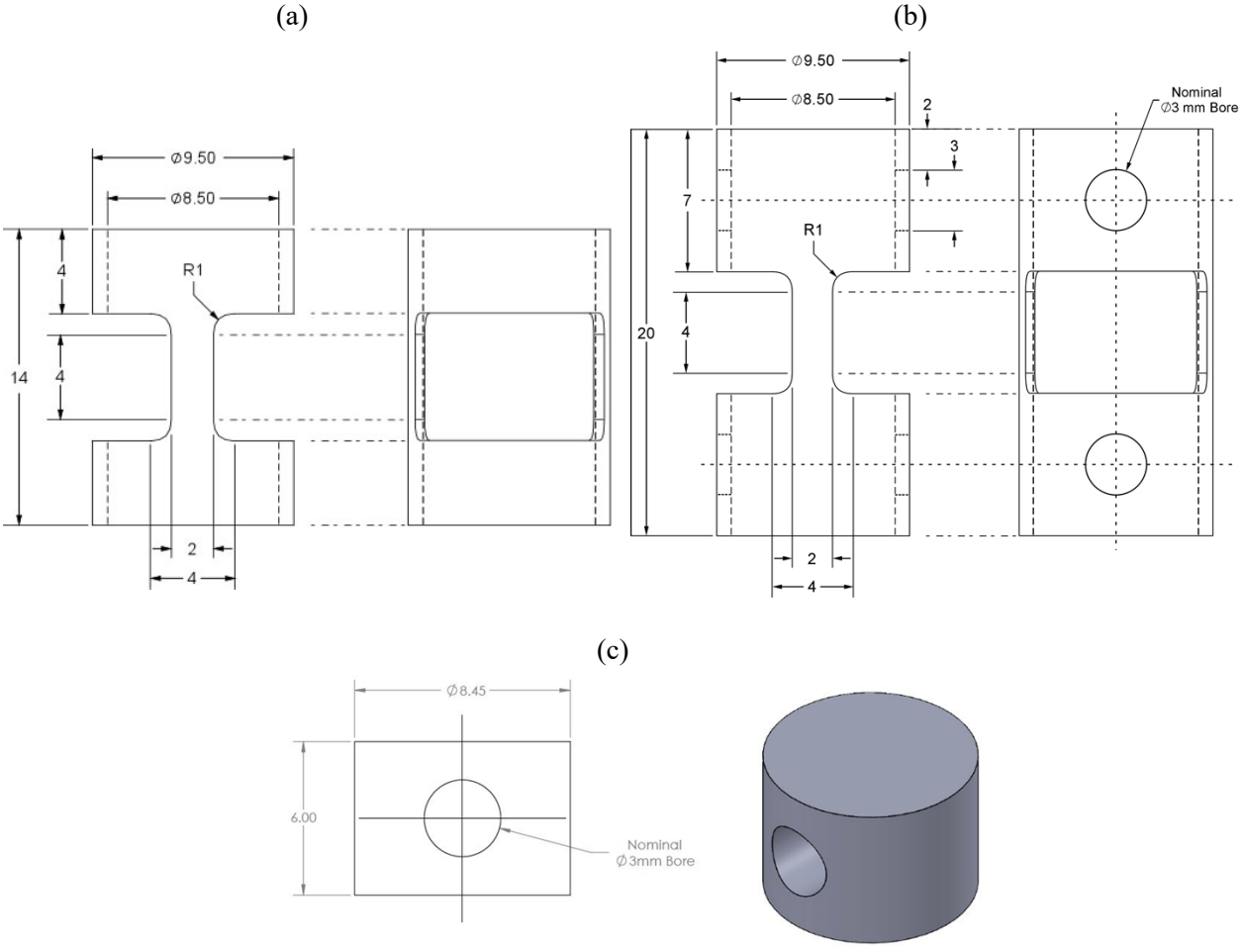

Figure 6. Design illustrations of the initial and modified dual-gauge axial specimen for the thin wall tube of C26M2. (a) initial design, (b) modified design and (c) plug for modified design.

Figure 7 shows digital images of two designs of the dual gauge axial specimens fabricated from the thin wall tube of C26M2. A total of 12 dual gauge axial specimens of the initial design and 38 dual gauge axial specimens of the modified design were fabricated. The fully assembled dual gauge axial specimen with the modified design is shown in Figure 7b. A total of 50 dual gauge ring specimens were fabricated.

(a) (b)

Figure 7. Digital images of each type of dual gauge specimens fabricated from the thin wall tube of C26M2. (a) initial design, (b) fully assembled modified design.

3.3 Creep Tests

3.3.1 Creep Concepts

Two types of creep tests were conducted in this study: 1) strain rate jump (SRJ) and 2) stress jump (SJ) and constant stress (CS). The two common parameters obtained from creep tests are the stress exponent (n) and activation energy for creep (Qc). The power law relationship shows the dependence of minimum, or secondary creep rate ($\dot{\varepsilon}_{\mathrm{m}}$) on stress ($\sigma$) and temperature (T)

$$\dot{\varepsilon}_{\mathrm{m}} = \mathrm{A}\sigma^{n}\exp\left(-\frac{Q_{\mathrm{c}}}{\mathrm{RT}}\right) \qquad \text{Equation 1}$$

where A is a material constant, n is the stress exponent and Q_{c} is the activation energy for creep. The values for A, n and Q_{c} vary with different creep mechanisms that are dominant in different regimes of stress and strain. The stress exponent is obtained from the SRJ tests while the activation energy for creep is obtained from both the SJ and CS tests. The material constant A was not obtained in this work but will be determined in future work with additional creep tests. To determine this constant, the minimum creep, or strain, rate is plotted against the applied stress on a log-log scale. The slope of the best fit to the results is the stress exponent and the intercept is the log A value.

Figure 8. illustrates how the creep properties obtained from the SRJ test correlate with that from the SJ and CS tests. Figure 8a shows the creep behavior of a specimen with constant stress. In primary creep (I), the strain rate increases rapidly and then slowly decreases as the specimen experiences work hardening. The specimen exhibits secondary creep (II) when the strain rate reaches a steady state (SS). Tertiary creep (III) shows an acceleration in the strain rate that ends with failure of the specimen. This type of creep behavior is observed in the constant stress test. In the jump stress test, the stress is increased after a reasonable amount of time for steady state creep rate is obtained that results in a new steady state creep rate regime. Figure 8b shows the creep behavior of a specimen with constant strain rate. The primary creep (I) shows a rapid increase in the stress that decreases due to hardening of the specimen. In secondary creep (II), the stress

remains constant with increasing time. The stress then decreases with time until failure of the specimen occurs in tertiary creep (III). This type of creep behavior is observed in the strain rate jump test, except that the strain rate is increased prior to specimen failure that causes the stress to increase further with time until the next constant stress regime is reached.

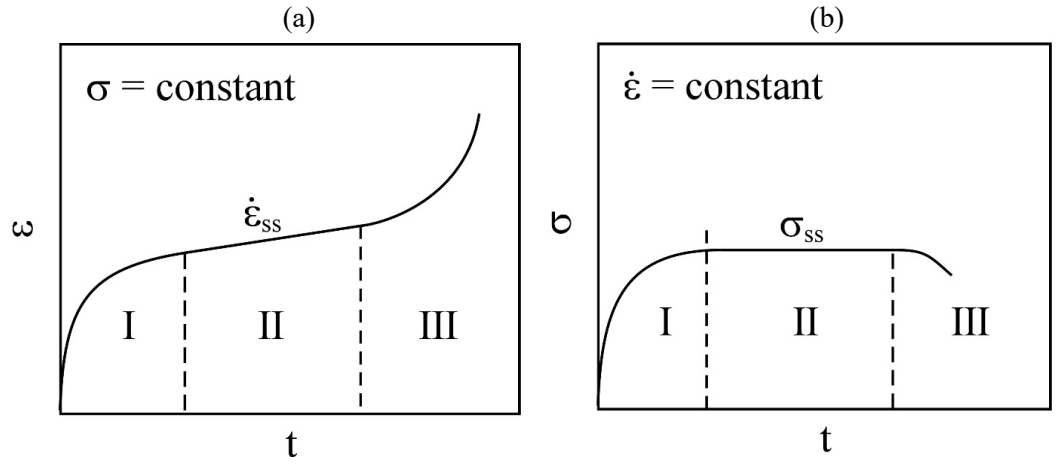

Figure 8. Plots illustrating the stress-strain curves for (a) creep tests using a constant stress and (b) creep tests using a constant strain rate.

3.3.2 Grips

Photographs of the grips used in the SRJ, SJ and CS tests with the dual gauge axial specimens and the ring pull test with the dual gauge ring specimens are shown in Figure 9. The grips for the dual gauge axial specimens shown in Figure 9a were fabricated from Rene 41 with 1 mm radius rounded edges for shoulder loading the axial specimens. The grips for the dual gauge ring specimens shown in Figure 9b were fabricated from Rene 41 with 0.79375 mm radius rounded edges for shoulder loading the rings specimens. The two half shaped mandrels were fabricated from Rene 41 and attached to the grips with screws.

Figure 9. The specimen grips used for the dual gauge axial specimens.

3.3.3 Test Frame

The SRJ, SJ and CS tests were performed on an Instron 4204 screw driven tensile machine with the Instron 5900R upgrade. An induction furnace is coupled to the Instron frame for rapidly heating the specimens to high temperature for tests. A reference thermocouple was spot welded to the lower end of the upper grip.

Figure 10 shows the typical set-up of an axial specimen in the grips for heating and testing. Figure 10a shows an axial specimen loaded in the grips with attached thermocouple inside the insulated Cu water cooled induction furnace coils. Figure 10b shows the ceramic shield placed over the axial specimen and grips prior to heating to the temperature. The heating rate of the induction furnace was rapid and typically reached the test temperatures as high as 900ºC in <7 minutes. It was desirable to achieve rapid heating to high temperatures to simulate the effects that heating rates have on the microstructure of C26M2 during an actual burst situation in a nuclear reactor. As soon as the test temperature was reached, the SRJ, SJ and CS tests were initiated. All tests were conducted in air.

3.3.4 Test Conditions

Table 2 lists the temperature, initial strain rate and value of stress obtained at the initial strain rate that were used in the strain rate jump tests on the dual gauge axial specimens. The initial strain rates are relatively high due in part to the minimum crosshead speed of the Instron 4203, which is 0.05 mm/minute, or 8.33×10^{-4} mm/second, which translates to the relatively high initial strain rates. The estimated strain rates determined from burst tests on FeCrAl cladding were ~2.58×10^{-3}/s at 677ºC and ~~1.00×10^{-2}/s at 777ºC and 877ºC [2]. These burst rates are comparable to the strain rates used in the strain rate jump tests shown in Table 2. The increase in initial strain rates at the highest temperatures compared to the lower temperatures is due to the low constant stresses measured with the initial strain rate. Table 3 lists the values of constant stress that were used at each temperature in the stress jump and constant stress tests.

(a) (b)

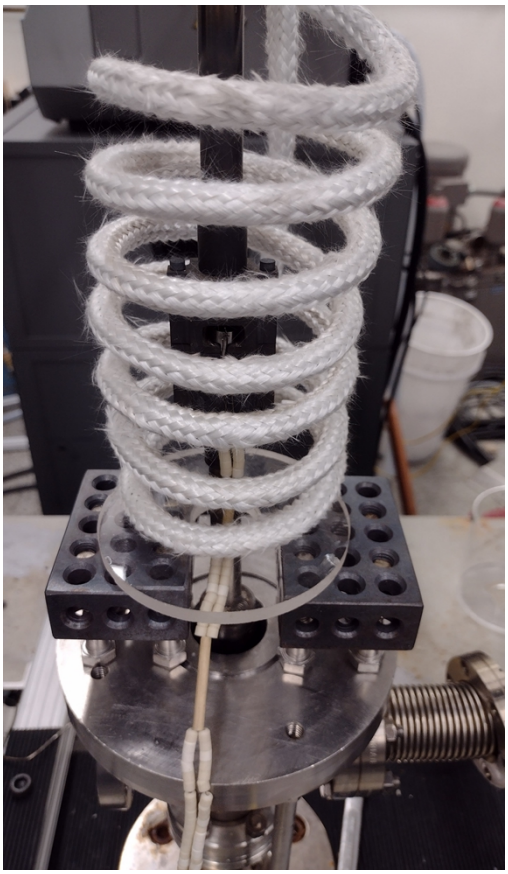

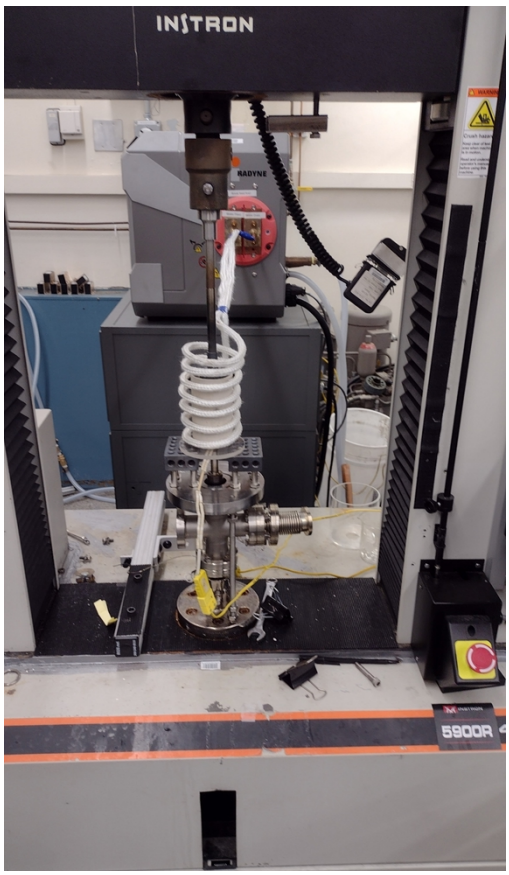

Figure 10. The set up of an axial specimen on the Instron 4204 tensile frame heated by induction furnace. (a) the axial specimen with the attached thermocouple loaded in the grips and (b) placement of the ceramic shield covering the axial specimen and grips prior to heating to the test temperature.

Table 2. Temperature, initial strain rate and stress value at the initial strain rate that were used in the strain rate jump tests on the dual gauge axial specimens.

Temperature	Initial strain rate	Stress at initial SR
(ºC)	(/s)	(MPa)
600	2.08×10^{-4}	147
700	4.00×10^{-4}	45
750	7.00×10^{-4}	42
800	2.00×10^{-3}	38
850	2.00×10^{-3}	37
900	4.00×10^{-3}	24

Table 3. The values of constant stress used at each temperature in the stress jump and constant stress tests on the dual gauge axial.

Temperature	Stress #1	Stress #2	Stress #3	Stress #4
(ºC)	(MPa)	(MPa)	(MPa)	(MPa)
750	-	15	20	25
800	10	15	20	25
850	10	15	20	25
900	10	15	20	25

3.4 Strain Rate Jump Tests

The concept of the strain rate jump test is illustrated in Figure 11 for the SRJ test on the axial specimen of C26M2 at 800ºC. At the start of the SRJ test the stress increases very slowly at the lowest strain rate that the Instron screw driven test frame could obtain until yielding occurs and the stress becomes nearly constant, or may reach a peak, with increasing strain (#1). After confirming the region of nearly constant stress with increasing strain, the strain rate was then increased, which is accommodated by an increase in stress to the next constant stress region (#2). These steps are repeated two more times with increases in strain rates (#3, #4 and #5). After starting the last strain rate increase, the axial specimen quickly yields and reaches the ultimate tensile stress followed by failure. The two gauges associated with the axial specimen may deform differently, which contributed to the noise in the stress-strain curves.

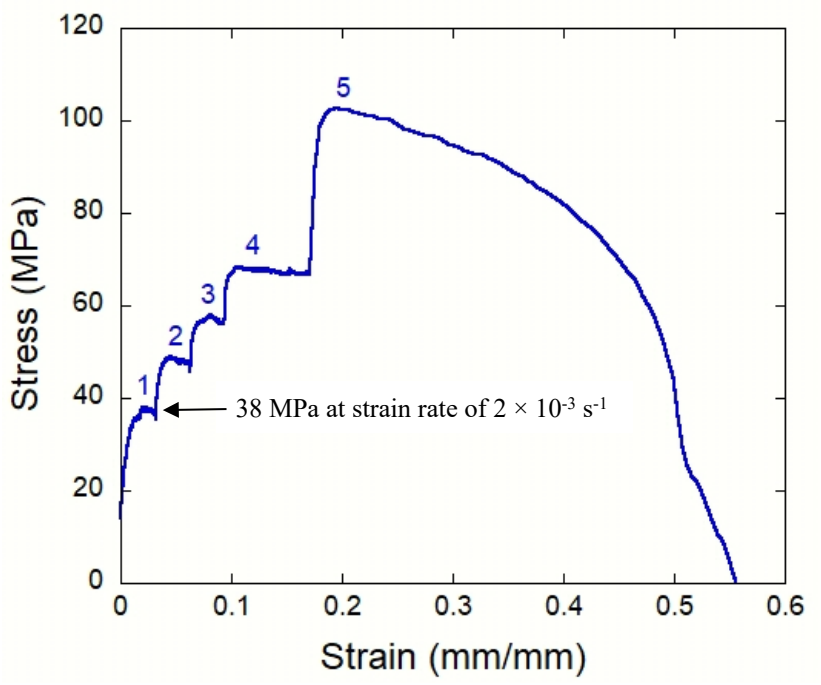

Figure 11. Stress-strain curve obtained from the SRJ test on the axial specimen of C26M2 at 800ºC.

The constant stress levels are measured at each temperature listed in Table 2 and used for calculating the stress exponent (n) in the power law relationship shown in equation 1. To obtain the stress exponent, the values of the log strain rate used in the SRJ test are plotted as a function of the measured values of log stress (σ) and the stress exponent is then determined from the following relationship:

$$n = \left(\frac{log\dot{\varepsilon}_m}{log\sigma}\right) \qquad \text{Equation 2}$$

where the slope obtained from the linear fit to the log values gives stress exponent.

3.5 Stress Jump and Constant Stress Tests

The stress jump test is illustrated in Figure 12 for the SJ test conducted on axial specimen of C26M2 at 800ºC. In a similar manner to the strain rate jump tests, at the start of the SJ test the lowest stress value is applied to the axial specimen. The strain increases initially at high strain rates that pertain to primary creep and then slowly decreases with time when strain changes nearly constant with time, which correlates with steady state creep rate, or secondary creep. After sufficient time occurs during steady state creep, the constant stress is then increased to the next higher level. In Figure 12, the constant stress level was initially 10 MPa and was then increased to 15 MPa followed by 20 MPa after sufficient times were obtained in the steady state creep regime. The red lines inserted in on the blue creep curve in Figure 12 shows the lengths of time and location of steady state creep regime that were used to estimate the creep rates for each stress at constant temperatures, which is determined from the slope of the line in the plot of strain rate as a function of time.

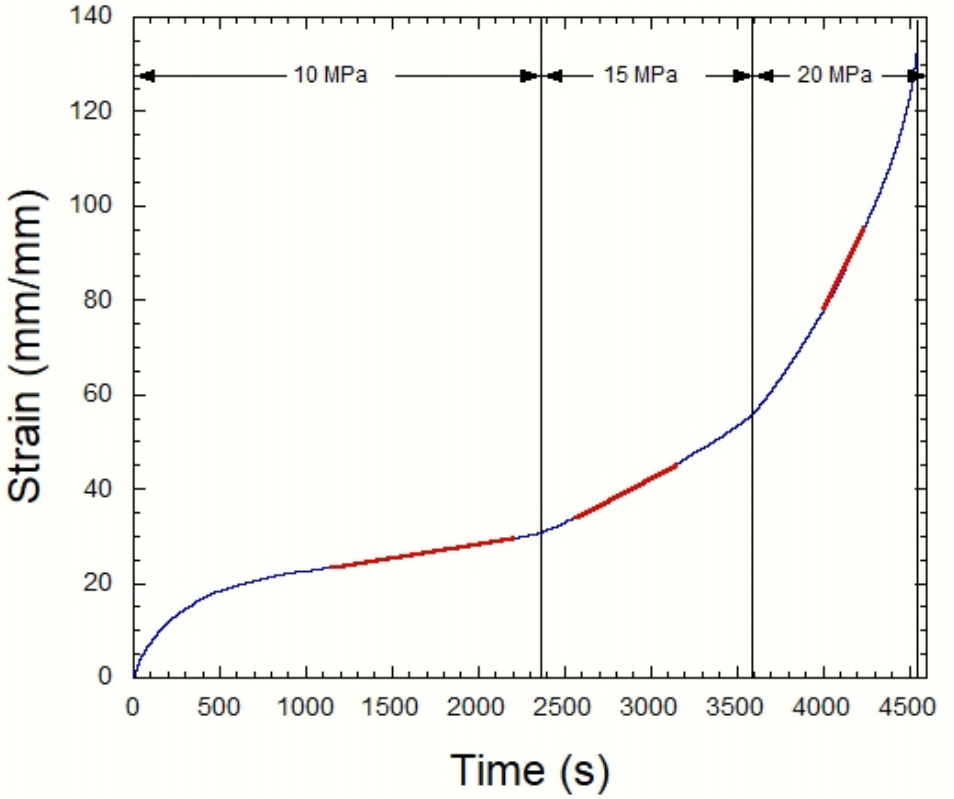

Figure 12. The stress jump test conducted on axial specimens of C26M2 showing the relationship between strain and time for each region of constant stress at 10, 15 and 20 MPa at 800ºC.

The constant stress test conducted on the axial specimen of C26M2 at 800ºC and 20 MPa is illustrated in Figure 13. In this test, a single constant stress was applied and the change in strain with time follows the three stages of creep illustrated in Figure 3.3.1a. The strain increases rapidly with time resulting in high strain rates during primary creep. The changes in strain rates slowly decreases until reaching the steady state creep rate during secondary creep. In constant stress tests at high temperatures and the higher constant stress conditions, tertiary creep occurs leading to a steady increase in strain rates until failure of the specimen occurs. For tests conducted at lower constant stress and temperature conditions, the constant stress test was terminated after sufficient time in secondary creep was reached since the initiation of tertiary creep may occur after very long times, which were out of scope for this study. The minimum creep rate during steady state creep was the only parameter that was required. The minimum creep rate was determined from the slope of the line in the plot of strain rate as a function of time for each test condition of stress and temperature.

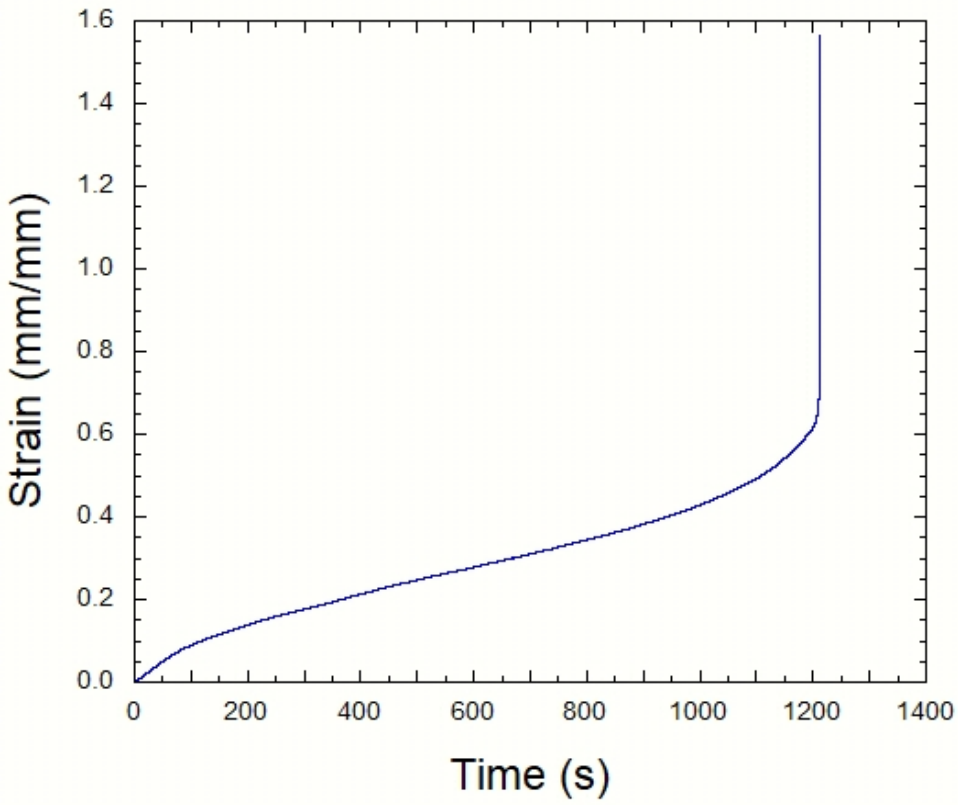

Figure 13. The constant stress test conducted on axial specimens of C26M2 showing the relationship between strain and time for constant stress at 800ºC and 20 MPa.

The steady state creep levels are measured at each constant stress listed in Table 3 and are used for calculating the activation energy of creep (Qc) in the power law relationship shown in equation 1. For the constant stress tests, the power law relationship of stress becomes:

$$\dot{\varepsilon}_{ss} = \mathrm{C}\exp\left(\frac{-\mathrm{Q}}{\mathrm{RT}}\right) \qquad \text{Equation 3}$$

Equation 3 can be linearized by taking natural logarithms of both sides:

$$\ln\dot{\varepsilon}_{ss} = \ln\mathrm{C} - \frac{\mathrm{Q1}}{\mathrm{RT}} \qquad \text{Equation 4}$$

A plot of $\ln\dot{\varepsilon}_{ss}$ as a function of $\frac{1}{\mathrm{T}}$ results in a linear relation with the slope $\frac{-\mathrm{Q}}{\mathrm{R}}$. The activation energy Q for creep is obtained by multiplying the slope with R, the universal gas constant (8.314 J/mole K).

4. RESULTS

4.1. Strain Rate Jump Tests

The creep properties obtained from the SRJ tests on the dual gauge axial specimens of C26M2 are shown in Figure 14. The values of the log strain rate ($\dot{\varepsilon}$) used in the SRJ tests are plotted against the measured values of the log stress (σ) as illustrated in Figure 11. The values of stress exponent (n) calculated from the slope of the linear fit to the log $\dot{\varepsilon}$ - log σ values is shown on the plot. The stress exponent values are obtained

from the slope of the linear fit and are shown on the plot. The results indicated that the highest stress exponent of n=5.8 occurs at 600ºC followed by the lowest stress exponent of n=2.5 at 700ºC. The values of stress exponents then increase slightly to a range of 2.9 to 4.3 between 750ºC and 900ºC. The high stress exponent value of 5.8 suggested dislocation creep mechanisms dominated creep deformation at 600ºC. The low stress exponent of 2.5 at 700ºC suggested diffusional creep mechanisms start to occur as well as dislocation cross-slip and climb mechanisms become easier. The slightly higher stress exponents of 2.9 to 3.9 may suggest different contributions of creep deformation mechanisms based on diffusional processes associated with Nabarro-Herring and Coble creep and dislocation creep that involve thermally activated cross-slip and climb mechanisms. However, these creep mechanisms could have been affected by early development of recovery and/or recrystallization processes in the microstructure of the C26M2 specimens.

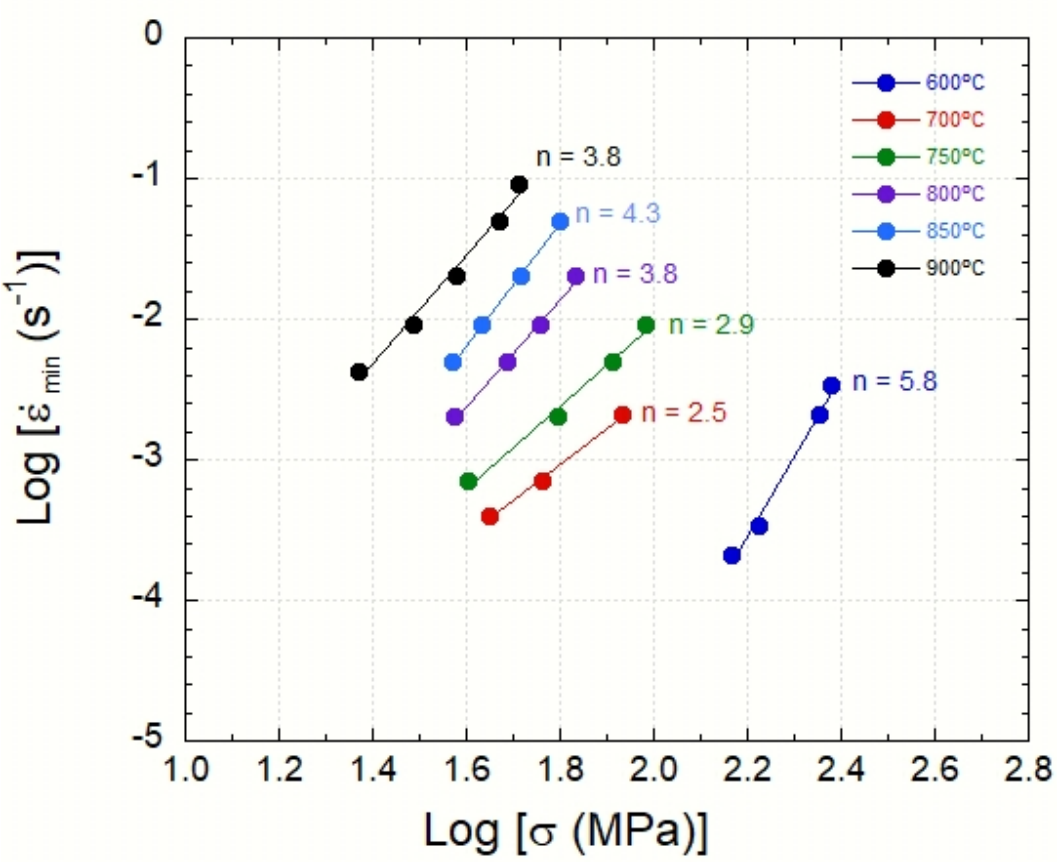

Figure 14. Comparison of the thermal creep behavior of 14YWT with OFRAC from SRJ tests conducted on axial specimens at 800ºC. The calculated stress exponents (n) are shown for each set of creep data.

After completing the SRJ test and recovering the broken axial specimen halves, it was observed that the circular shape of the axial specimen prior to the SRJ test had deformed to an elliptical shape. The magnitude of the deformation was noticeable for tests in the range 700ºC to 900ºC. Figure 15 shows digital images of the gauge heads following the SRJ tests at the test temperatures of 700ºC and 900ºC. The maximum distortions occurred on opposite ends of the gauge head where the gauges are located. The loading characteristics on the axial specimens by the grips during the SRJ test depends on the contact area between the gauge head and the surface of the grip. During the SRJ test at high temperatures, the stress concentration on the two gauges will exert forces on the contact surface area between the gauge head and grip, which may lead to stresses on the gauge heads by the grips that leads to the distortions. This distortion may increase the uncertainty in the results but it likely affects the magnitude of strain more than that of the measured stress.

(a) (b)

Figure 15. Digital images of the gauge sections of the axial specimens following the SRJ tests. (a) 600ºC and (b) 900ºC.

4.2 Stress Jump and Constant Stress Tests

The initial creep tests using the stress jump method illustrated in Figure 12 for determining the activation energy of creep were conducted using the initial design of the dual gauge axial specimens shown in Figure 6a. Similar to the SRJ tests, these axial specimens also deformed to the elliptical shape during stress jump tests. The stress jump tests were conducted with 3 stresses of 10, 15 and 20 MPa at 800ºC, 850ºC and 900ºC. These test conditions permitted the calculation of 3 creep activation energies for C26M2. Figure 16 shows the data plotted as ln MCR (measured minimum creep rate) as a function of 1/T (K^{-1}). The slope fit to the data at each stress provides the activation energy (Q_c). Surprisingly, the lowest Q_c value of 173.8 KJ/mole was observed with the stress of 20 MPa.

The lowest stress of 10 MPa showed a slightly higher Q_c value of 188.2 KJ/mole followed by the highest Q_c value of 214.7 KJ/mole. The high MCR value measured at 20 MPa and 850ºC does not agree well with the linear fit through the other two values of MCR and was suspect. Similar to this observation, the MCR at 15 MPa and 20 MPa may be suspect as well. Unfortunately, these 3 stress jumps consumed the last of the dual gauge axial specimens with the initial design and no further stress jump tests could be performed to verify the suspect MCR values.

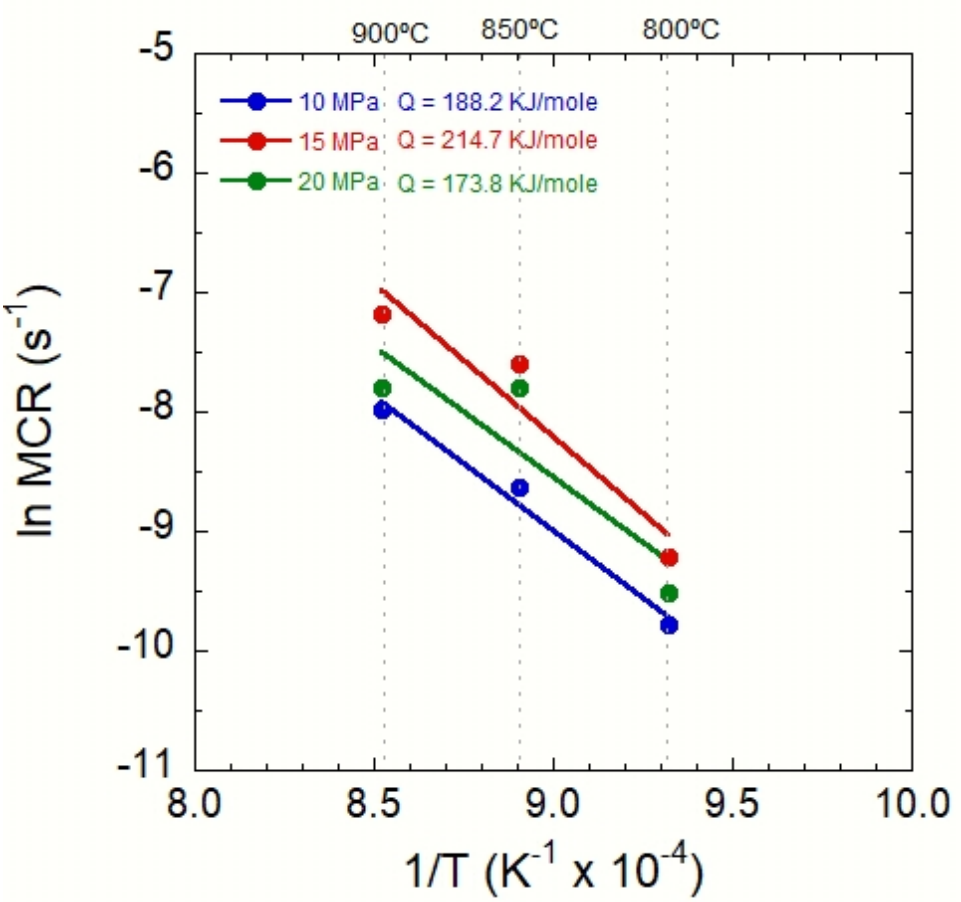

Figure 16. Results of the stress jump tests conducted at stresses of 10, 15 and 20 MPa for temperatures of 800ºC, 850ºC and 900ºC.

Following the stress jump testing method, there was concern that the microstructure of the C26M2 axial specimens may softened during the time allowed for obtaining the steady state creep rate that could have had an effect on the steady state creep rate obtained at the next higher constant stress. Microstructure softening would lead to higher steady state creep rates than would be expected if a single constant stress was used. Based on this concern, each test condition used in the stress jump test was reevaluated with single constant stress tests so that any microstructural softening only during the test. In addition, the constant stress (CS) tests were conducted using the modified dual gauge axial specimens with screws attaching tube wall to each plug as illustrated in Figure 6. After each constant stress test was completed, no distortion of the axial gauge head was observed so that the plug achieved the goal of eliminating this issue.

The constant stress tests were conducted with 4 stresses of 10, 15, 20 and 25 MPa at 750ºC, 800ºC, 850ºC and 900ºC. These test conditions permitted the calculation of 4 creep activation energies for C26M2. Figure 17 shows the data obtained by constant stress tests plotted as ln MCR (measured minimum creep rate) as a function of 1/T (K^{-1}). The results show steady increases in MCR with increasing temperature at each stress, which is expected. The slope fit to the data at each stress provides the activation energy (Q_c). The best linear fit to the MCR values at each stress was with data obtained at 800ºC, 850ºC and 900ºC. The MCR values obtained at 750ºC show significant deviation from the linear fits indicating a different creep mechanisms involving Coble creep and Nabarro-Herring creep more dominant. Unlike the results obtained from jump stress tests, the lowest Q_c value of 130.8 KJ/mole was observed with the highest stress of 25 MPa. As stress was lowered, the Q_c values increased continuously to the highest value of 188.2 KJ/mole at 10 MPa. This

trend suggests that the dominant creep mechanism is diffusional based dislocation climb since the decreasing activation energies with increasing stress promotes easier dislocation climb around obstacles.

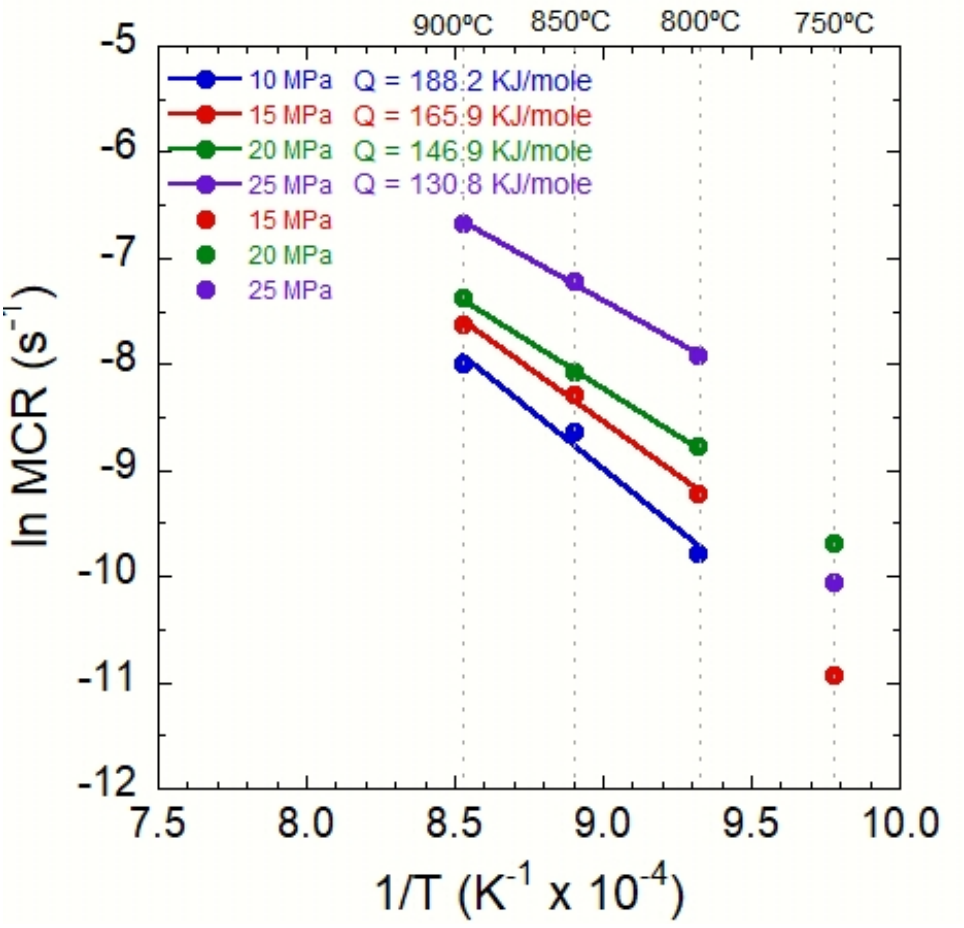

Figure 17. Results of the constant stress tests conducted at stresses of 10, 15, 20 and 25 MPa for temperatures of 750ºC, 800ºC, 850ºC and 900ºC.

4.3 Accuracy of the Creep Testing Methods

Although the strain rate jump (SRJ) and stress jump test (SJ) methods have been used in published studies, it is still important to question the accuracy of the results especially since the geometry of the subsize dual gauge axial specimen is not common and also to the challenges with performing these tests at very high temperatures that are not intended for use of the FeCrAl C26M2 alloy. Tensile tests conducted on C26M showed considerable decreases of >66% in yield and ultimate tensile stresses from room temperature to 600ºC and further decrease to below 100 MPa at 700ºC up to 800ºC [2].

Therefore, one question that arises is whether softening of the microstructure occurs during the SJ test that may influence the MCR after increasing the constant stress. The single constant stress (CS) tests does not have this issue and may be considered to be more accurate in obtaining values for creep activation energies. Figure 18 compares the minimum creep rate values obtained from SJ and CS tests at 800ºC, 850ºC and 900ºC. At all three temperatures the results show higher creep rates from the SRJ tests compared to the CS tests. Therefore, the creep activation energies calculated from the CS data and shown Figure 17 are more representative of the creep properties of C26M2 at these high temperatures.

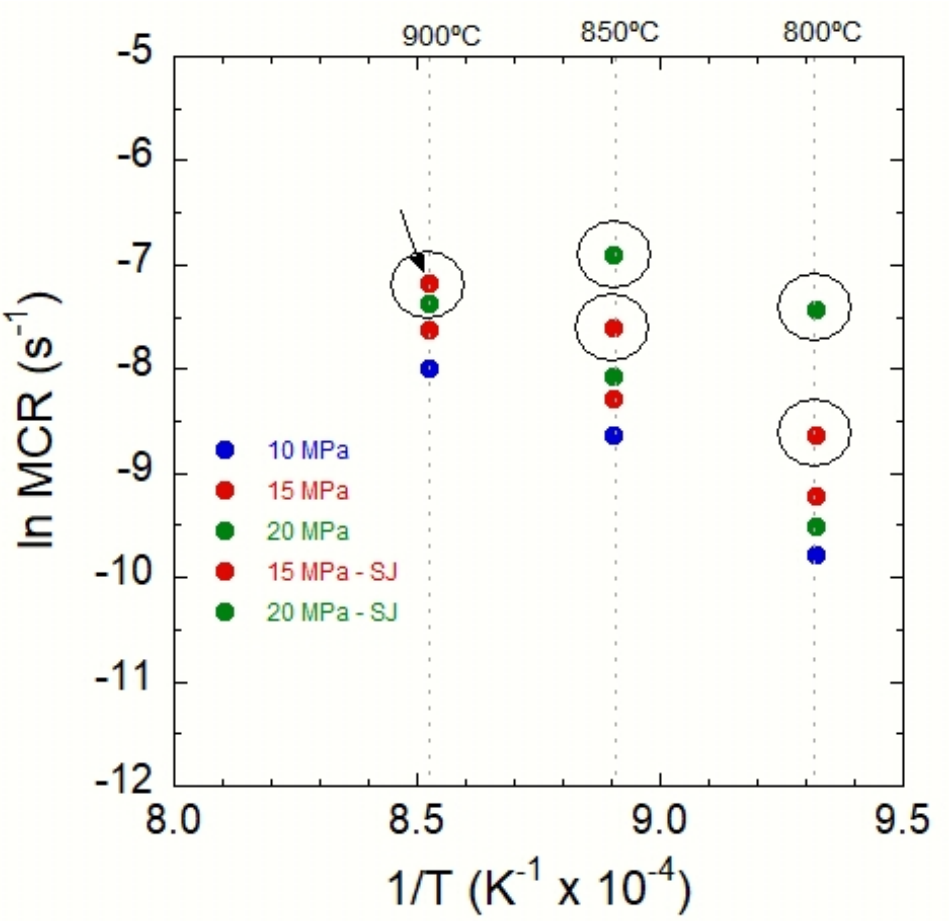

Figure 18. Comparison of the MCR values obtained from the constant stress tests and the stress jump tests (enclosed open circles and black arrow for 15 MPa in SJ test) for stresses of 10, 15 and 20 MPa for temperatures of 800ºC, 850ºC and 900ºC.

Another question is whether microstructural softening occurs during the SRJ test that may influence the stress measured after each increase in strain rate. Figure 19 compares the stress exponents obtained from the SRJ tests and the stress exponents obtained from the MCR measurements in the CS tests. The 3 stress exponents determine from MCR values in the singe CS tests are lower than those obtained from the SRJ tests, although the stresses obtained in the SRJ tests were generally higher compared to the CS tests. However, at 900ºC, a similar stress of ~25 MPa was obtained at the lowest strain rate used in the SRJ test and the highest constant stress used in the single CS tests. Yet the MCR value for the CS test in much lower than the strain rate value for the SRJ test at 900ºC. This indicates that the stress exponents calculated from the CS data give a better representation of the creep properties of C26M2 at these high temperatures.

Based on these two comparison of results, the best type of creep test that should be performed at high temperatures on FeCrAl alloys such as C26M2 is the single CS test. It should also be noted that the modified dual gauge axial specimen used in the CS tests added to the accuracy of the creep results since no distortions occurred with gauge head.

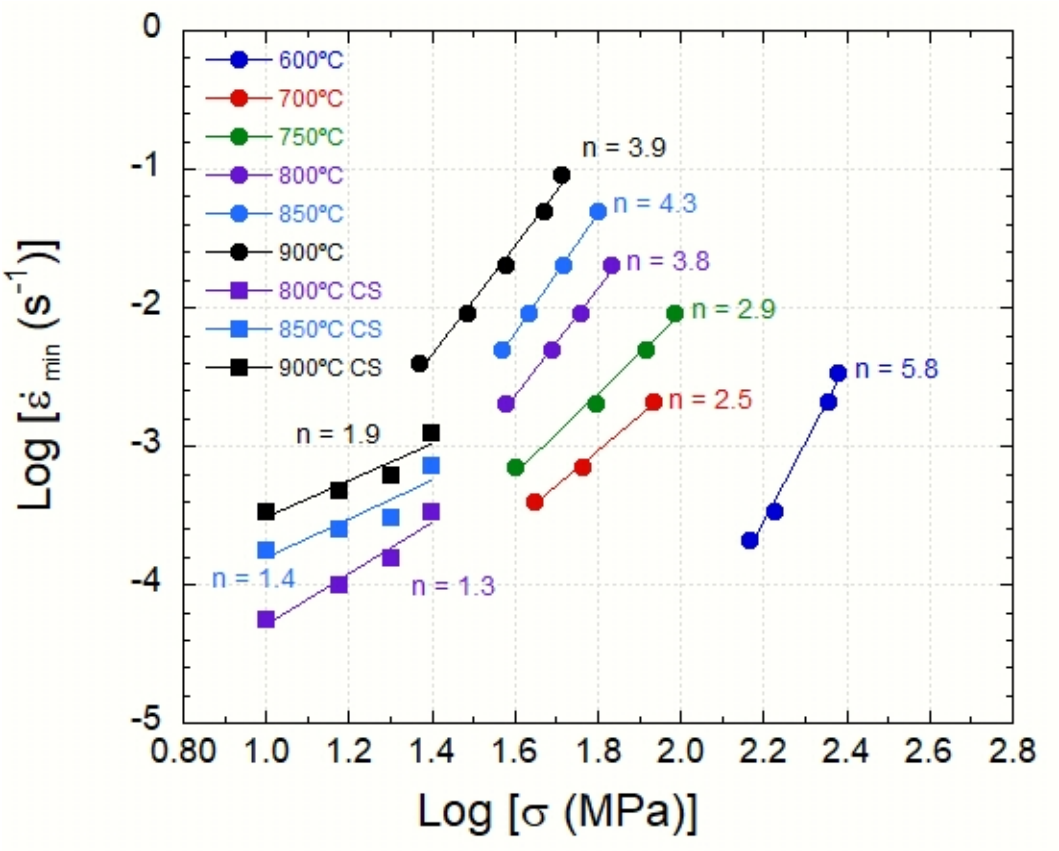

Figure 19. Compilation of the stress exponents obtained from the strain rate jump tests over the temperance range of 600ºC to 900ºC and the MCR values measured in the constant stress tests 800ºC, 850ºC and 900ºC.

Finally, for evaluating and implementing the values of n and Q_c obtained from the SRJ and CS tests in this work into a fuel performance code, Tables 4 and 5 show the test conditions and the appropriately measured data for determining the n and Q values, respectively. For calculation of stress exponent (n) in Table 4, for the SRJ tests, the test temperature and strain rate parameters that were used and the constant stress values that were measured, and for the CS test, the test temperature and single constant stress parameters that were used and the minimum creep rate values that were measured are listed. In Table 5, the minimum creep rate that was measured at 800ºC, 850ºC and 900ºC for each constant stress that were used for calculation of the activation energy of creep (Q_c) are listed. Regardless of the test method, at high temperatures of 800ºC, 850ºC and 900ºC, the creep rates are high and approach the strain rates used in typical tensile tests and the stresses responsible for high creep rates are small, which demonstrate the rapid deformation that fuel cladding of C26M2 experiences in these temperature and stress regimes.

Table 4. Test parameters that were used and the values of either constant stress (SRJ) or steady state creep rate (CS) that were measured for calculation of the stress exponent (n).

Temperatures	Test Method	Strain Rate (SRJ) or Minimum Creep Rate (CS)	Stress	Stress Exponent
(ºC)	(SRJ or CS)	(/s)	(MPa)	(n)
600	SRJ	2.08×10^{-4}	147	5.8
		3.35×10^{-4}	168	
		2.08×10^{-3}	226	
		3.35×10^{-4}	239	
700	SRJ	4.00×10^{-4}	45	2.5
		7.00×10^{-4}	58	
		2.08×10^{-3}	86	
750	SRJ	7.00×10^{-4}	42	2.9
		2.00×10^{-3}	62	
		5.00×10^{-3}	82	
		9.00×10^{-3}	96	
800	SRJ	2.00×10^{-3}	38	3.8
		5.00×10^{-3}	49	
		9.00×10^{-3}	57	
		2.00×10^{-2}	68	
850	SRJ	5.00×10^{-3}	37	4.3
		9.00×10^{-3}	43	
		2.00×10^{-2}	52	
		5.00×10^{-2}	63	
900	SRJ	4.25×10^{-3}	24	3.8
		9.00×10^{-3}	31	
		2.00×10^{-2}	38	
		5.00×10^{-2}	47	
		9.00×10^{-2}	52	
800	CS	5.66×10^{-5}	10	1.3
		9.98×10^{-5}	15	
		1.55×10^{-4}	20	
		3.37×10^{-4}	25	
850	CS	1.79×10^{-4}	10	1.4
		2.53×10^{-4}	15	
		3.10×10^{-4}	20	
		7.33×10^{-4}	25	
900	CS	3.40×10^{-4}	10	1.9
		4.85×10^{-4}	15	
		6.31×10^{-4}	20	
		1.26×10^{-3}	25	

Table 5. Test parameters for the single constant stress (CS) tests and the values of minimum creep rate (CS) that were measured for calculation of the activation energy of creep (Q_c).

Stress	Temperature	Minimum Creep Rate	Activation Energy
MPa	(ºC)	(/s)	(KJ/mole)
10	800	5.66×10^{-5}	188.2
	850	1.79×10^{-4}	
	900	3.40×10^{-4}	
15	800	9.97×10^{-5}	165.9
	850	2.53×10^{-4}	
	900	7.64×10^{-4}	
20	800	1.55×10^{-4}	146.9
	850	3.10×10^{-4}	
	900	6.31×10^{-4}	
25	800	3.36×10^{-4}	130.8
	850	7.32×10^{-4}	
	900	1.27×10^{-4}	

5. SUMMARY

The creep behavior of C26M2 was investigated at stresses and temperatures that lead to cladding bursts for FeCrAl alloys. The creep properties that were obtained consisted of stress exponents using SRJ tests and creep activation energies using SJ and single CS tests. The SRJ tests were conducted from 600ºC to 900ºC while the SJ and CS tests were conducted from 800ºC to 900ºC. Form the SRJ tests, the results indicated that the highest stress exponent of 5.8 occurred at 600ºC that then decreased to the lowest stress exponent of 2.5 at 700ºC. At higher temperatures, the stress exponents increased slightly to a range of 2.9 to 4.3 between 750ºC and 900ºC. The high stress exponent value of 5.8 suggested dislocation glide mechanisms dominated creep deformation at 600ºC since high constant stress values were measured. The low stress exponent of 2.5 at 700ºC suggested diffusional creep mechanisms start to occur as well as dislocation cross-slip and climb mechanisms become easier. The slightly higher stress exponents of 2.9 to 3.9 may suggest different contributions of creep deformation mechanisms based on diffusional processes associated with Nabarro-Herring and Coble creep and dislocation creep that involve thermally activated cross-slip and climb mechanisms. These deformation mechanisms could have also been affected by the development of recovery and/or recrystallization processes in the microstructure of the C26M2 specimens. From the SJ and single CS tests, two sets of creep activation energies were calculated. The steady state creep values obtained from the SJ tests showed several abnormalities especially with the data at 850ºC. The comparison of the creep activation energies between the data from the SJ and CS tests showed higher creep rates for the SJ tests than for the CS tests, indicating microstructure softening occurred in the C26M2 specimens during the SJ tests that led to the higher creep rates at stresses above the initial stress of 10 MPa. For the CS tests, the results showed steady increases in MCR with increasing temperature at each stress. The best linear fit to the MCR values at each stress was with data obtained at 800ºC, 850ºC and 900ºC. The lowest Q_c value of 130.8 KJ/mole was observed with the highest stress of 25 MPa. As stress was lowered, the Q_c values increased continuously to the highest value of 188.2 KJ/mole at 10 MPa. This trend suggests that the dominant creep mechanism is diffusional based dislocation climb since the decreasing activation energies with increasing stress promotes easier dislocation climb around obstacles. The comparison between the SJ and CS tests indicates that the best type of creep test performed on FeCrAl alloys such as C26M2 is the single CS test.

6. FUTURE WORK

The future work on C26M2 will consist of doing a limited number of tests using single strain rates with the axial specimens at the high temperatures to compare the stress exponents determined by these tests with those obtained from the SRJ tests to assess the accuracy of the results. Further single CS tests well be conducted on the axial specimens at lower temperatures to calculate the material constant A in equation 1 for the power law relationship. Single CS tests will begin with the dual gauge ring specimens fabricated from the thin wall tube of C26M2. The results obtained with future work on accuracy of n and Q_c values will be incorporated into Bison and validating the FeCrAl burst test.

7. REFERENCES

1. C.P. Massey, K.A. Terrani, S.N. Dryepondt and B.A. Pint, *Cladding burst behavior of Fe-based alloys under LOCA*, Journal of Nuclear Materials, **470** (2016) 128-138.
2. K.A. Gamble, T. Barani, D. Pizzocri, J.D. Hales, K.A. Terrani, G. Pastore, *An investigation of FeCrAl cladding behavior under normal operating and loss of coolant conditions,* Journal of Nuclear Materials **491** (2017) 55-66.
3. S.B. Bell, K.A. Kane, C.P. Massey, L.A. Baldesberger, D. Lutz, B.A. Pint, *Strength and rupture geometry of un-irradiated C26M FeCrAl under LOCA burst testing conditions*, Journal of Nuclear Materials, **557** (2021) 153242 (1-13).

4 R.T. Sweet, C.P. Massey, S.B. Bell, K.A. Kane, *Wrought FeCrAl Alloy (C26M) Cladding Behavior During Burst Experiments and Performance Under LOCA Conditions*, TopFuel 2022, Raleigh, NC.

5. K.A. Terrani, T.M. Karlsen and Y. Yamamoto, *Input Correlations for Irradiation Creep of FeCrAl and SiC Based on In-Pile Halden Test Restults*, Report: ORNL/TM-2016/191, (2016).
6. P. Joshi, B. Kombaliah, M.N. Cinbiz and K.L. Murty, Characterization of stress-rupture behavior of nuclear grade C26M2 FeCrAl alloy for accident-tolerant fuel cladding via burst testing, Materials Science and Engineering A, 791 (2020) 139753 (1-22).